Journal of Experimental Botany, Vol. 72, No. 4 pp. 1336–1348, 2021
doi:10.1093/jxb/eraa508 Advance Access Publication 1 November 2020
This paper is available online free of all access charges (see https://academic.oup.com/jxb/pages/openaccess for further details)

RESEARCH PAPER

Potassium content diminishes in infected cells of *Medicago truncatula* nodules due to the mislocation of channels MtAKT1 and MtSKOR/GORK

Elena E. Fedorova[1,*], Teodoro Coba de la Peña[2,3], Victoria Lara-Dampier[2], Natalia A. Trifonova[1], Olga Kulikova[4], José J. Pueyo[2] and M. Mercedes Lucas[2,*]

[1] K. A. Timiryazev Institute of Plant Physiology, Russian Academy of Science, Moscow, Russia
[2] Instituto de Ciencias Agrarias ICA-CSIC, Madrid, Spain
[3] Centro de Estudios Avanzados en Zonas Áridas (CEAZA), La Serena, Chile
[4] Wageningen University, Wageningen, The Netherlands.

* Correspondence: elenafedorova06@mail.ru or mlucas@ica.csic.es

Received 18 July 2020; Editorial decision 13 October 2020; Accepted 3 December 2020

Editor: Miriam Gifford, University of Warwick, UK

Abstract

Rhizobia establish a symbiotic relationship with legumes that results in the formation of root nodules, where bacteria encapsulated by a membrane of plant origin (symbiosomes), convert atmospheric nitrogen into ammonia. Nodules are more sensitive to ionic stresses than the host plant itself. We hypothesize that such a high vulnerability might be due to defects in ion balance in the infected tissue. Low temperature SEM (LTSEM) and X-ray microanalysis of *Medicago truncatula* nodules revealed a potassium (K^+) decrease in symbiosomes and vacuoles during the life span of infected cells. To clarify K^+ homeostasis in the nodule, we performed phylogenetic and gene expression analyses, and confocal and electron microscopy localization of two key plant Shaker K^+ channels, AKT1 and SKOR/GORK. Phylogenetic analyses showed that the genome of some legume species, including the *Medicago* genus, contained one SKOR/GORK and one AKT1 gene copy, while other species contained more than one copy of each gene. Localization studies revealed mistargeting and partial depletion of both channels from the plasma membrane of *M. truncatula* mature nodule-infected cells that might compromise ion transport. We propose that root nodule-infected cells have defects in K^+ balance due to mislocation of some plant ion channels, as compared with non-infected cells. The putative consequences are discussed.

Keywords: AKT1, GORK, *Medicago truncatula*, potassium channels, SKOR, symbiosis, symbiosome, X-ray microanalysis

Introduction

The symbiotic relationship of soil bacteria, collectively known as rhizobia, with leguminous plants is the source of the ammonia produced from atmospheric nitrogen by the symbiosomes (Roth and Stacey, 1989), the form of rhizobia housed in infected cells of root nodules.

Nodules are more sensitive to stresses, such as salt and heavy metals, in comparison with the roots of the host plant and the plant itself. These stresses are detrimental for nodule formation and nitrogen-fixing activity (Zahran, 1999; Tsyganov *et al.*, 2007; Shvaleva *et al.*, 2010; Coba de la Peña and Pueyo,

2012; Bertrand *et al.*, 2016). Although such abiotic stresses have an effect on the plant ionome, and the high vulnerability of the nodule might be due to defects in ion balance in the infected tissue, a comprehensive model of plant–microsymbiont ion homeostasis in legume nodules has not yet been established.

One of the essential ions involved in plant adaptive responses to abiotic stresses is potassium (K^+) (Wu *et al.*, 2018; Rubio *et al.*, 2020). It is a macronutrient involved in the control of osmotic status and turgor, cation/anion balance, control of membrane polarization, cytoplasmic pH regulation, cell expansion, and organ movements, such as stomatal aperture (Karnik *et al.*, 2017; Ragel *et al.*, 2019).

The availability of K^+ for the cell depends on transport, ion voltage, and concentration of K^+ on both sides of the membrane. K^+ transport is expected to oscillate between uptake and loss over periods of tens of seconds to many minutes (Wang and Wu, 2013; Shabala and Potosin, 2014; Ragel *et al.*, 2019). Plant K^+ transporters have defined functions in K^+ uptake or release, storage in vacuoles, and ion translocation between tissues and organs (Wang and Wu, 2013; Ragel *et al.*, 2019). Regarding legume nodulation, some K^+ transporters were identified in root hair transcriptomes of *Lotus japonicus*, *Glycine max*, and *Medicago truncatula*, and have been proposed to be involved in the early stages of nodulation (Desbrosses *et al.*, 2004; Damiani *et al.*, 2016; Rehman *et al.*, 2017). However, information about K^+ transport in nodules is really scarce (Benedito *et al.*, 2010; Udvardi and Poole, 2013; Drain *et al.*, 2020).

AKT1 is one of the main K^+-permeable channels (Coskun and Kronzucker, 2013; Véry *et al.*, 2014). In *Arabidopsis thaliana*, the Shaker-type channel AtAKT1, located in the plasma membrane, has been shown to mediate both high- and low-affinity K^+ acquisition in roots (Sharma *et al.*, 2013). The so-called plant Shaker family is a group of voltage-gated K^+ channels. The structure of a Shaker-type K^+ protein subunit consists of six transmembrane domains close to the N-terminus, a pore domain (involved in voltage sensing) located between the fifth and sixth transmembrane domains, an acyclic nucleotide monophosphate-(cNMP) binding domain involved in channel activation potential, several repeated ankyrin domains involved in protein–protein interactions and signal transduction, and a dimerization domain (KHA) located at the C-terminal end. Functional K^+ channels are tetramers of this protein subunit (Wang and Wu, 2013; Nieves-Cordones *et al.*, 2014; Véry *et al.*, 2014).

Outward-rectifying channels mediate K^+ release and open at depolarized membrane potentials; this group is composed of SKOR and GORK channels in *A. thaliana* (Ragel *et al.*, 2019). SKOR is involved in K^+ transport from root stellar cells into the xylem and from roots to shoots, while GORK is expressed in the epidermis and functions in K^+ release (Gaymard *et al.*, 1998; Demidchik, 2014). According to the data of Long-Tang *et al.* (2018), constitutively overexpressed melon SKOR has a positive effect on growth and improves saline tolerance in *A. thaliana*. Recently, it was shown that only one gene of an outward Shaker K^+ channel is present in the genome of *M. truncatula* (Drain *et al.*, 2020). These authors analysed the functional activity of this channel. They have shown that this channel poorly contributed to K^+ translocation towards the shoots, but was quite important in the membrane outward K^+-permeable conductance in leaf guard cells. Hence, this channel showed the functional features of a GORK channel, and it was designated by Drain *et al.* (2020) as MtGORK. However, this channel is annotated as MtSKOR in the NCBI database, so we are using a double name MtSKOR/GORK to prevent confusion.

In the present study, to investigate the ion compartmentalization in the symbiotic tissue, we have performed an ion distribution analysis (IDA) of *M. truncatula* root nodules by low temperature SEM (LTSEM) and X-ray microanalysis. The analysis was mainly focused on vacuoles of the nodule tissues and symbiosomes. In the nodule-infected zone, K^+ content decreased in the vacuoles of infected cells and in symbiosomes during the life span of the infected cell. This suggests that K^+ homeostasis could be impaired in infected cells.

To clarify the decrease of K^+ content observed during the life span of the infected cells, we analysed two key plant Shaker K^+ channels with opposite K^+ transport vectors: the inwardly rectifying K^+ channel AKT1 (MtAKT1) and the Stellar K^+ outward rectifier channel SKOR/GORK (MtSKOR/GORK). Differences in the location of both channels were found between infected and non-infected nodule cells. In infected cells, mistargeting and partial depletion of both channels in the plasma membrane occurred before K^+ decrease in the vacuole. We propose that the maintenance of the intracellular bacterial colony might have an effect on the K^+ availability for the host cell. Root nodule-infected cells might have defects in K^+ balance due to the differences/flaws in the location of MtAKT1 and MtSKOR/GORK, as compared with non-infected cells. Our results provide new insights into infected cell development and location of the K^+ channels MtAKT1 and MtSKOR/GORK in nodules.

Materials and methods

Plants, bacteria, and growth conditions

Medicago truncatula Gaertn. cv. Jemalong A17 plants were grown according to Limpens *et al.* (2004). *Agrobacterium rhizogenes* strain MSU440 was used for hairy root transformation (Limpens *et al.*, 2004). *Sinorhizobium meliloti* strain Sm2011 or *S. meliloti* Sm2011-mRFP expressing the monomeric red fluorescent protein (mRFP) were used for nodulation (Smit *et al.*, 2005).

Ion distribution analysis (IDA)

IDA was performed with a Zeiss DSM-960low temperature scanning electron microscope with energy-dispersive spectrometry and X-ray microanalysis (Pentaflet, Oxford, UK). Twenty-eight days post-inoculation (dpi), nodules were collected and immediately frozen. The nodules were fractured via the long axis to reveal all the developmental zones, and immediately analysed. For the IDA, an accelerating voltage of 20 kV, a resolution of 133 eV, and a spot acquisition method were used. Quantitative element analysis was obtained by using standard ZAF (atomic number, absorption, and fluorescence) correction procedures with Link Isis, version 3.2 (Oxford, UK). The high resolution of LTSEM permits the estimation

of the ion content in individual plant organelles and cell structures (Leidi *et al.*, 2010). We targeted the symbiosomes and vacuoles in the developmental zones, that were distinguished by their position inside the nodules. The comparison was done between the same structures (symbiosomes or vacuoles) from different nodule developmental zones. For each analysis, 10 nodules were used, 10–15 cells were analysed per nodule, and 7–12 symbiosomes and vacuoles were examined.

Accession numbers or gene identifiers

MtAKT1 (MTR_4g113530) and *MtSKOR/GORK* (MTR_5g077770). The homologue *M. truncatula* genes *MtAKT1* and *MtSKOR/GORK* were identified using the available genomic and cDNA sequence databases utilizing the *A. thaliana* sequences for BLAST search.

Phylogenetic and protein sequence analyses

MtSKOR/GORK and *MtAKT1* nucleotide and protein sequences and homologues in other legume species were retrieved from several databases and plant genomic resources: National Centre for Biotechnology Information (https://www.ncbi.nlm.nih.gov/), Phytozome (https://phytozome.jgi.doe.gov/pz/portal.html), the Legume Information System (https://legumeinfo.org/), the White Lupin Genome site (https://www.whitelupin.fr/), the pea genome project (https://urgi.versailles.inra.fr/Species/Pisum), and the *Lotus japonicus* genome assembly site (http://www.kazusa.or.jp/lotus). *Arabidopsis thaliana AKT1*, *GORK*, and *SKOR* sequences were used as queries.

Phylogenetic analyses of *AKT1* and *SKOR/GORK* homologue genes of several legume species were performed by using the maximum likelihood method. The Tamura–Nei model (Tamura and Nei, 1993) and general time reversible model (Nei and Kumar, 2000) were used for AKT1 and SKOR/GORK analyses, respectively. Node robustness was assessed by the bootstrap method (n=1000 pseudoreplicates). Evolutionary analyses were conducted in MEGA X (Kumar *et al.*, 2018).

Protein domains were predicted with the SMART tool (http://smart.embl-heidelberg.de/). Putative protein transmembrane domains were predicted with the Phyre2 Web portal prediction and analysis tool (http://www.sbg.bio.ic.ac.uk/~phyre2/html/page.cgi?id=index; Kelley *et al.*, 2015). Multiple protein sequence alignment was performed with Clustal Omega (https://www.ebi.ac.uk/Tools/msa/clustalo/).

Plasmid constructs and plant transformation

The *MtAKT1* ORF and its 2.5 kb regulatory sequence were amplified via PCR from nodule cDNA and genomic DNA, respectively, using Phusion high-fidelity polymerase (Finnzymes).

MtAKT1 and *MtAKT1* putative promoters were directionally cloned into a pENTR-D-TOPO plasmid (Invitrogen). The Gateway cloning system (Invitrogen) was used to create genetic constructs for *promoter:GUS* (β-glucuronidase) and *GFP* (green fluorescent protein) fusions. pENTR-D-TOPO carring *MtAKT1* was recombined using Gateway LR Clonase II (Invitrogen) into the Gateway destination vector pKGW-GGRR by LR reaction to create the *ProMtAKT1:GUS* fusion. To make the *ProMtAKT1:MtAKT1:GFP* translational fusion, *MtAKT1* was cut out from pENTR-D-TOPO with restriction enzymes *Not*I and *Asc*I, purified from a gel, and ligated into pENTR 4, 1 digested with *Bsa*I. Afterwards, pENTR constructions containing *ProMtAKT1* and *MtAKT1* and pENTR 2, 3 containing GFP were introduced by multisite LR recombination into the Gateway destination vector pKGW-MGW. All primers used are listed in Supplementary Table S1.

RNA extraction and gene expression analysis

Nodules at 28 dpi were collected and dissected into three parts: the white apical zone containing meristem (M) and the infection zone (z2), the medial red part (young and mature nitrogen fixation zone) (z3), and the basal part, which included the senescent zone (z4).

Total RNA was extracted from nodules using the E.Z.N.A. RNA Plant Mini Kit (Omega Bio-Tek, Norcross, GA, USA) and retro-transcribed into cDNA using the iScript cDNA Synthesis Kit (Bio-Rad). Expression analysis of *MtAKT1* and *MtSKOR/GORK* was performed by real-time quantitative PCR (qPCR). The constitutively expressed *Mtc27* and *MtGAPDH* genes were used as endogenous controls (Coba de la Peña *et al.*, 2008; Verdier *et al.*, 2008). Gene-specific primers were designed using the PRIMER 3-PLUS software (Untergasser *et al.*, 2007) and with Primer Express v3.0 software (Applied Biosystems, Foster City, CA, USA). The real-time PCRs were performed on a 7300 Real Time PCR System (PE Applied Biosystems) using SYBR Green Supermix (Bio-Rad). The comparative C_T method (Pfaffl, 2001) or the standard curve method (Torres *et al.*, 2014) were applied for relative quantification. All primers used are listed in Supplementary Table S1.

Localization of gene expression by GUS staining

Transgenic roots and nodules were collected, washed in 0.1 M sodium phosphate buffer, pH 7.2, incubated in GUS buffer under vacuum at room temperature for 30 min, and incubated at 37 °C for 2 h for the enzymatic reaction. Roots and hand-sectioned nodules were photographed using a Nikon Optiphot-2 microscope.

Confocal microscopy

A Leica MZFLIII fluorescence microscope with filter cubes for GFP (excitation, 470/40 nm; dichroic, 495 nm; emission, 525/50 nm) and DsRed (excitation, 545/30 nm; emission, 620/60 nm) was used for the selection of transgenic tissue.

Confocal imaging was done on hand-sectioned nodules with a Zeiss LSM 5 Pascal confocal laser-scanning microscope (Carl Zeiss) and a Meta LSM 510 microscope in a single image mode.

Nodules were fixed in 1% formaldehyde, cut along the longitudinal axis, and blocked with 2% BSA. The GFP signal in the sections carrying *ProMtAKT1:MtAKT1:GFP* constructs was enhanced by using an antibody (Ab) against GFP developed in rabbit (Molecular Probes) at 1:50 dilution.

For double immunolabelling of MtAKT1 and Rab7, anti-GFP rabbit Ab was mixed with anti-Rab7 Ab developed in mouse (Limpens *et al.*, 2009), followed by addition of the secondary Abs anti-rabbit CY3 Ab (excitation maximum 548 nm, emission maximum 561 nm; Molecular Probes) and anti-mouse Alexa 488 (excitation maximum 490 nm, emission maximum 525 nm; Molecular Probes), respectively. For immunolocalization of MtSKOR/GORK, a custom-made Ab developed in rabbit (GenScript) from the peptide sequence FHPWDPKEQRRNGI [peptide–keyhole limpet haemocyanin (KLH) conjugate] was used in a 1:100 dilution. An anti-rabbit Alexa 488 Ab (excitation maximum 490 nm, emission maximum 525 nm; Molecular Probes), diluted 1:200, was used as secondary Ab.

The comparative estimation of the relative intensity of the fluorescence signal was performed by ImageJ multipoint analysis of brightness (Schneider *et al.*, 2012). Analysis of the signal for MtAKT1 and MtSKOR/GORK in infected and non-infected cells was performed on 10 cells for each group on the same set of green channel Tiff images obtained by confocal microscopy; each sampling contained 45 points.

Electron microscopy

Transgenic nodules carrying the *ProMtAKT1:MtAKT1:GFP* construct were fixed and embedded in Lowicryl K4M (Fedorova *et al.*, 1999). EM grids with the samples were blocked with 2% BSA and incubated overnight at 4 °C with the primary Ab anti-GFP developed in rabbit

(Molecular Probes) at 1:50 dilution, followed by colloidal 10 nm gold-conjugated goat anti-rabbit Ab (BioCell).

For the localization of MtSKOR/GORK, wild-type nodules fixed and embedded as described above were used. The immunolocalization was carried out with the custom-made Ab developed in rabbit (GenScript) at a dilution of 1:50, followed by colloidal 10 nm gold-conjugated goat anti-rabbit Ab (BioCell).

Samples were analysed using a LIBRA120 electron microscope (Carl Zeiss).

Purification of plasma membrane

Purification of plasma membrane from the roots of 5-day-old *M. truncatula* seedlings was performed by the method of aqueous two-phase partitioning (Hodges and Mills, 1986).

The seedling roots were homogenized in 100 mM Tris–HCl buffer at pH 8 in the presence of 300 mM sucrose, 10 mM EDTA, 5 mM $K_2S_2O_5$, 5 mM DTT, and 1 mM phenylmethylsulfonyl fluoride (PMSF; 1/2 w/v) at 4 °C, filtered through a cotton cloth, and centrifuged at 10 000 *g* for 15 min. The obtained supernatant was centrifuged at 186 000 *g* for 40 min, the precipitate was resuspended in buffer consisting of dextran T500 and polyethylene glycol 3350 supplemented with 0.3 M sucrose, 3 mM KCl, 0.1 mM EDTA, and 1 mM DTT, and centrifuged at 2500 rpm for 5 min. The upper phase of the phase separation gradient, which contains the plasma membrane, was centrifuged at 186 000 *g* for 40 min. The precipitate containing the plasma membrane proteins was used for western blot analysis.

Western blot analysis

The proteins from the precipitate of the plasma membrane were resuspended in 0.025 M Tris–HCl buffer containing 1 mM EDTA, 1 mM DTT, and protease inhibitor cocktail (Roche). A 75 µg aliquot of protein was loaded per well. The proteins were separated by 12% SDS–PAGE and were blotted to a nitrocellulose membrane (Bio-Rad). The membrane was incubated in 3% BSA, as a blocking agent, followed by primary anti-SKOR-specific Ab, at a 1:50 dilution, followed by the secondary Ab anti-rabbit immunoglobulin G peroxidase produced in goat (Sigma), at a 1:5000 dilution. The immunosignal was revealed by incubation with the Immuno-Star Western chemiluminescent kit (Bio Rad). Blots were photographed with a Molecular Imager Chemi Doc XRS+, using Image Lab software in Chemi mode. The pre-stained protein ladder was photographed in normal light.

Statistical methods

IDA was performed twice from two separate experiments. Ten nodules from different plants per experiment were used. Measurements were performed for infected and non-infected cells; 10–15 cells from each nodule were analysed. Gene expression analysis was performed twice from two separate experiments. The Student test was used to determine the significance of the difference between the means of data sets.

Results

Ion compartmentalization in nodule cells

IDA was performed on root nodules fractured along the long axis to reveal all developmental zones (Fig. 1A). *Medicago truncatula* nodules have a developmental gradient of cells in an apical–basal direction from the apical meristem to the zone of senescence (Vasse *et al.*, 1990). Proximal to the nodule meristem (M) is positioned the infection zone (z2), where bacteria are released from infection threads. Next to z2 is the nitrogen fixation zone (z3), which consists of large infected cells and small non-infected cells. The basal part of the nodule (z4) contains senescent infected cells. The cortex surrounding the central part of the nodule consists of non-infected cells only. High magnification was used to distinguish individual symbiosomes and vacuoles (Fig. 1B).

Distribution of K^+, sodium, magnesium, phosphorus, chlorine, calcium, iron, copper, and molybdenum was analysed (Fig. 1C; Supplementary Table S2). The major difference detected in the cells of the infected zone, according to the IDA, was in K^+ content, which significantly diminished during the life span of infected cells (Fig. 1C). The level of K^+ was lower in symbiosomes in mature and senescent infected cells than in young infected cells. In the young symbiosomes, the K^+/Na^+ ratio was ~5, while in mature and senescent symbiosomes, this ratio diminished until it reached 1. Vacuoles of infected cells in the senescent zone also showed a lower score for K^+ ions than those in young and mature infected cells. The vacuoles of non-infected cells from the inner and outer cortex and from the central part of the nodule did not show significant differences in K^+ content (Fig. 1C). Vacuoles of nodule cortex cells showed differences in sodium, chlorine, and calcium content compared with vacuoles of non-infected cells situated in the infected zone (Supplementary Table S2).

Our results suggest that K^+ transport may be altered during the life span of infected cells; therefore, we decided to study two of the main K^+ channels in the plant cell plasma membrane, an inwardly rectifying K^+ channel (AKT1) and an outward-rectifying channel that mediates K^+ release from cells (SKOR).

Phylogenetic analyses

A phylogenetic analysis of *A. thaliana AKT1* putative homologues of several legumes was performed. Legume homologues that formed a clade with *A. thaliana AKT1* are shown in Fig. 2A. It was observed that some legume species (*M. truncatula*, *Pisum sativum*, *Trifolium pratense*, *Cicer arietinum*, *Lotus japonicus*, *Cajanus cajan*, *Vigna* sp., *Phaseolus vulgaris*, and *Arachis duranensis*) have just one *ATK1* homologue in a single locus in their genomes, whilst the genomes of other species (*Glycine* sp., *Lupinus* sp., and *Arachis hypogaea*) contain two homologues, in two different loci (Fig. 2A).

Phylogenetic analysis of putative *SKOR/GORK* gene homologues of several legumes was also performed. The genomes of *A. thaliana* and other Brassicales (*Brassica rapa* and *Capsella rubella*) contain one *SKOR* gene homologue and one *GORK* gene homologue, that were included in the phylogenetic inference. The obtained phylogenetic tree displayed two differentiated clades of legume *SKOR/GORK*-like homologues (designated as 'legume homologues clade I' and 'legume homologues clade II' in Fig. 2B). Legume homologues in clade I clustered with Brassicales SKOR and GORK genes. *SKOR/GORK* legume homologues clade I contained one or

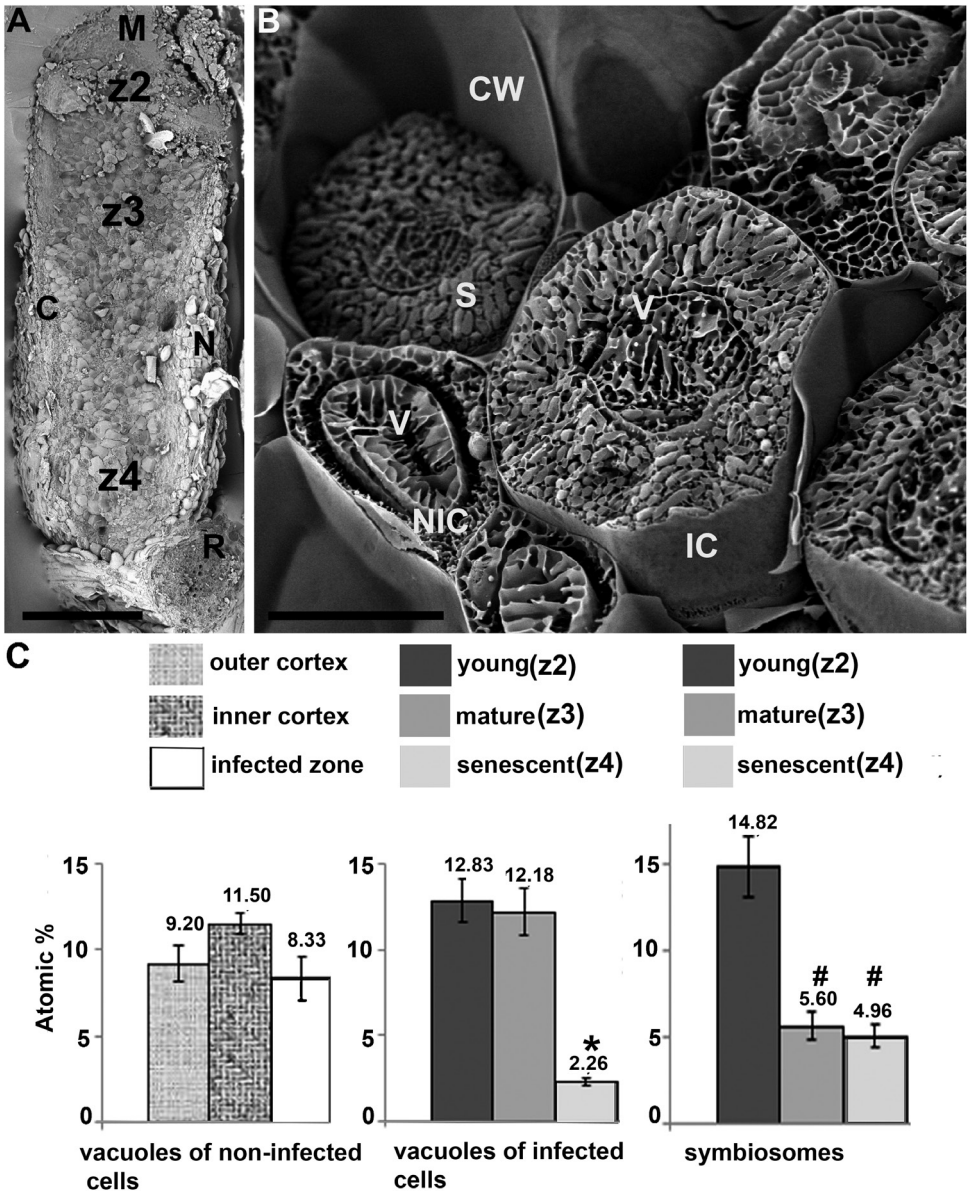

Fig. 1. (A, B) LTSEM images of *M. truncatula* nodules and potassium distribution. (A) Image of a freeze-fractured nodule and root of *M. truncatula*. (B) High magnification of infected and non-infected cells. (C) Relative distribution of K^+ in vacuoles and symbiosomes in the different nodule zones for nodules prepared by LTSEM. The elemental analysis was carried out focusing the excitation X-ray beam into the vacuoles or the symbiosomes exposed in fractured cells. The number and the energy of the X-rays re-emitted from the specimens were measured by an energy-dispersive spectrometer. Data represent means ±SD of atomic (%) (n=10–13). * indicate significant differences between infected cell vacuoles in z2, and in z3 and z4; # indicate differences between symbiosomes in z2, and in z3 and z4. C, cortex zone, CW, cell wall; IC, infected cell; N, nodule; NIC, non-infected cell; R, root; S, symbiosome; V, vacuole; M (zone1), meristem; z2, young infected zone; z3, mature infected zone; z4, senescent zone. Scale bars: (A) 500 μm; (B) 50 μm.

two genes (corresponding to one or two loci) per genome, with the same relationship between species and number of loci observed for *AKT1* homologues. An exception was *Lupinus albus*, as three genes were identified in its genome; two of them (Lalb_Chr17g0346031 and Lalb_17g0346021) were located next to each other in the same chromosome and putatively code for shorter proteins (Fig. 2B).

SKOR/GORK legume homologues clade II contains other *SKOR/GORK*-like genes identified in *C. cajan*, *Vigna* sp., *Glycine* sp., and *Arachis* sp., but not found in the genomes of the other studied legume species (Fig. 2B).

Sequence analyses of legume homologues of potassium channels AKT1, SKOR, and GORK

Sequence analysis showed that both *M. truncatula* homolog proteins MtAKT1 and MtSKOR/GORK contained a voltage-dependent K^+ channel domain, a cNMP-binding

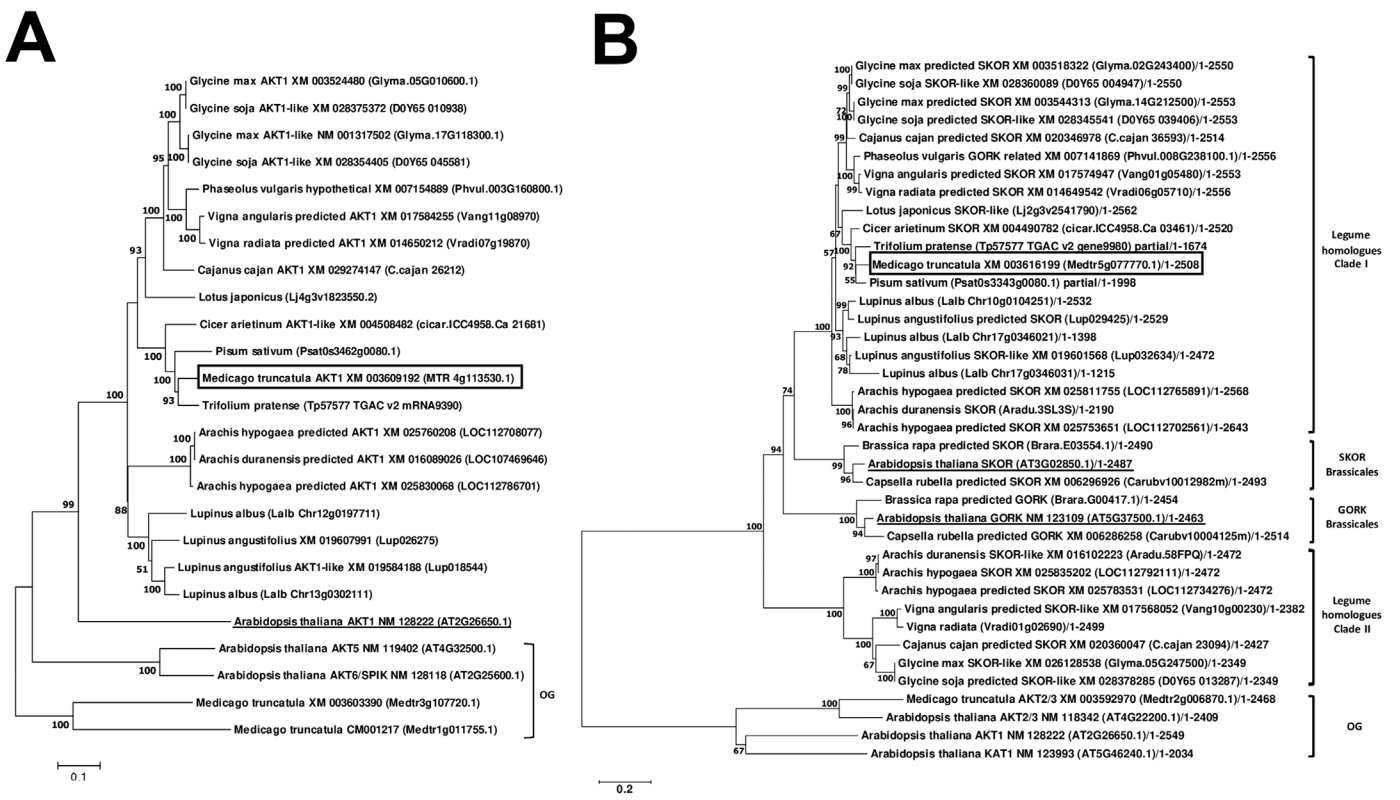

Fig. 2. Evolutionary analyses of *AKT1* and *SKOR/GORK* homologues of *M. truncatula* and other legumes. (A) The evolutionary history of *AKT1* was inferred by using the maximum likelihood method and Tamura–Nei model. A discrete Gamma distribution was used to model evolutionary rate differences among sites. The tree with the highest log likelihood is shown. The *M. truncatula AKT1* reference gene is contained in a box. The *A. thaliana AKT1* reference is underlined. *Arabidopsis thaliana AKT5*, *AKT6*, and two *M. truncatula* homologue sequences were added as the outgroup (OG). (B) Evolutionary history of *SKOR/GORK* homologues in *M. truncatula* and other legumes was inferred by using the maximum likelihood method based on the general time reversible model. A discrete Gamma distribution was used to model evolutionary rate differences among sites. The tree with the highest log likelihood is shown. The *M. truncatula* reference gene is contained in a box. *Arabidopsis thaliana GORK* and *SKOR* references are underlined. Clusters containing legume and Brassicales homologues are identified to the right. The *A. thaliana AKT1*, *AKT2/3*, *KAT1*, and *M. truncatula AKT2/3* gene sequences were added as the OG. In both trees, bootstrap values are shown next to the branches (1000 pseudoreplicates). The trees are drawn to scale, with branch lengths measured in the number of substitutions per site. For each gene, the GenBank accession number and/or gene name (in parentheses) are indicated.

domain, several repeated ankyrin (ANK) domains involved in signal transduction, and a dimerization domain rich in hydrophobic and acidic residues (KHA) located at the C-terminus (Supplementary Fig. S1A, B). Both proteins also contained six transmembrane domains (S1–S6), which are also characteristic of these Shaker K^+ channel proteins (Supplementary Figs S2A, S3A). MtAKT1, MtSKOR/GORK, and their corresponding homologues identified in other legume species also have the pore loop domain (P) between S5 and S6, harboring the GYGD hallmark motif, present in P domains of highly selective K^+ channels (Supplementary Figs S2B, S3B) (Lebaudy *et al.*, 2007; Drain *et al.*, 2020). Both AtSKOR and AtGORK legume homologues also display two conserved amino acid residues (M, V) of the P loop and two residues (D, M) in S6 that are involved in the dependency of the channel voltage-sensitive gating on the external K^+ concentration (Fig. S3B) (Johansson *et al.*, 2006; Drain *et al.*, 2020). A particular case is that of *L. albus*, with three SKOR/GORK homologues. Two of them (Lalb_Chr17g0346031 and Lalb_17g0346021) are shorter proteins, one of them containing the transmembrane domain and voltage-dependent K^+ channel domain, and the other containing the cNMP, ANK, and KHA domains.

Expression analysis of potassium channels in nodules

An analysis was performed by qPCR from RNA extracted from 28 dpi nodules dissected in three parts: white meristem plus infection zone (M/z2), red middle nitrogen-fixing zone (z3), and basal senescence zone (z4) (Fig. 3A, B). The expression levels of *MtAKT1* and *MtSKOR/GORK* showed no significant differences among the analysed nodule zones.

Promoter:GUS expression analysis of *AKT1* in root showed its expression in meristematic cells, cortex, and vascular bundles (Fig. 3C). In nodule primordia, expression was detected over the whole organ (Fig. 3D). Mature nodules showed a uniform distribution of expression throughout the nodule (Fig.

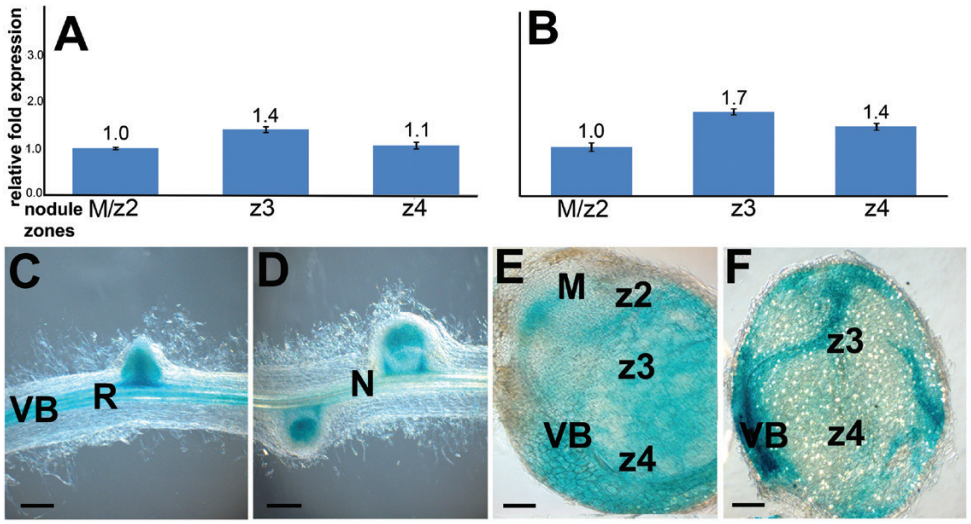

Fig. 3. *MtAKT1* and *MtSKOR/GORK* expression in nodules. (A, B) Relative transcription of *MtAKT1* (A) and *MtSKOR/GORK* (B) in the different nodule developmental zones as analysed by qPCR. Data represent means ±SD (n=3). (C–F) Histochemical staining of GUS activity in the transgenic roots and nodules carrying the construct *ProAKT1:GUS* (C) Root and root primordium. Expression detected in vascular bundles and meristem. (D) Nodule promordium and young root nodule. Expression in the meristematic region and in the zone of cell growth. (E) Developed nodule showing expression in all nodule zones. (F) Senescing nodule. Expression was detected in all nodule developmental zones and vascular bundles. R, root primordium; M, meristem; N, nodule primordium; VB, vascular bundles; z2, infection zone; z3, nitrogen-fixing zone; z4, senescence zone. Scale bars: (C–F) 100 µm.

3E) and, in senescent nodules, expression was mainly detected in vascular bundles (Fig. 3F). *Promoter:GUS* expression analysis of *MtSKOR:GORK* was recently reported by Drain *et al.* (2020). The analysis showed gene expression throughout the nodule and in vascular bundles of the root.

Localization of MtAKT1 and MtSKOR/GORK proteins in infected and non-infected cells using confocal and electron microscopy

MtAKT1 was located in the plasma membrane of meristematic cells, non-infected cells along the nodule developmental zones, and infected cells in the infection zone (Fig. 4A, B). In mature infected cells, packed with symbiosomes, the plasma membrane labelling was quite low, in contrast to non-infected cells (Fig. 4C). MtAKT1 signal was mainly detected in the cytoplasm in a dotted pattern and was partly depleted from the plasma membrane (Fig. 4C; Table 1; Supplementary Fig. S4).

The specificity of the anti-MtSKOR/GORK Ab was tested by western blot. In plasma membrane isolated from *M. truncatula* roots, anti-SKOR Ab recognized a band of 95.99 kDa, the expected size for MtSKOR/GORK protein (Supplementary Fig. S5). In nodule cells, MtSKOR/GORK signal was detected in both the plasma membrane and the symbiosome membrane (Fig. 4D, F; Supplementary Fig. S4). In mature infected cells, the protein was depleted from the plasma membrane similarly to MtAKT1 (Fig. 4E; Table 1).

With the aim to characterize the observed dot-like signal, we performed a double localization analysis of MtAKT1 and the small GTPase Rab7, which is a marker for late endosomes/vacuoles (Limpens *et al.*, 2009). According to the analysis, the MtAKT1 signal partially (24%) co-localized with Rab7 (Fig. 4G). Hence, this result indicated that part of MtAKT1 protein was internalized from the plasma membrane by endosomes similar to the cycles of turnover of the Shaker channel KAT1 in stomatal cells (Meckel *et al.*, 2004), but most of the dot-like signal might be located in other organelles.

To resolve the dot pattern observed by confocal microscopy, immunogold EM was performed. According to the analysis, the immunogold signal for MtAKT1 and MtSKOR/GORK was detected in the endoplasmic reticulum and plasma membrane (Fig 5A, B). The immunogold EM analysis of MtSKOR/GORK confirmed the data of confocal microscopy and showed that MtSKOR/GORK was also associated with the symbiosome membrane (Fig. 5B).

The comparative estimation of fluorescence intensity over the plasma membrane regions of infected and non-infected cells demonstrated the partial depletion of both channels from the plasma membrane of infected cells (Table 1).

Discussion

The root nodule is a temporary organ with a short life span. The co-existence of symbionts is usually described as mutually beneficial for both of them (Wang *et al.*, 2018). However, the infected cells have a short life span in comparison with non-infected root cells (Puppo *et al*, 2005), and the inevitable scenario of symbiosome lysis and death of the host cell after 12–18 d of existence has been well described (Kijne, 1975; Yang *et al.*, 2017).

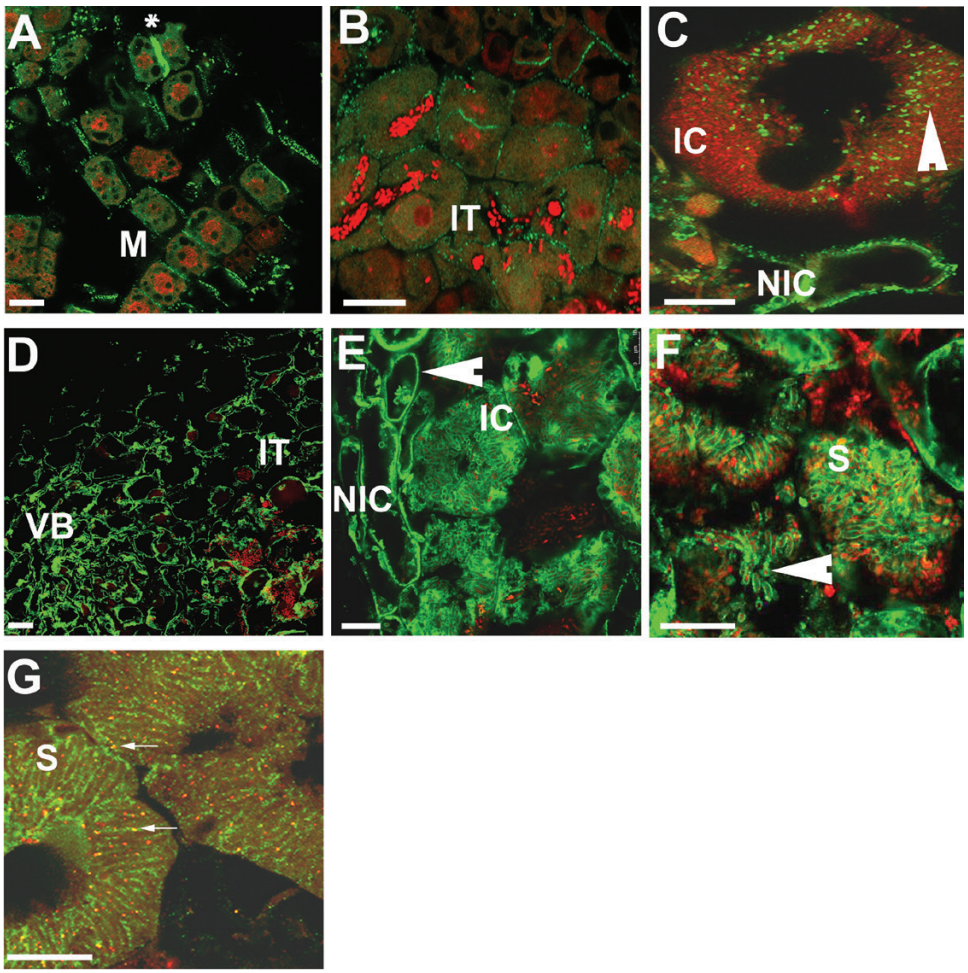

Fig. 4. Localization of the potassium transporters MtAKT1 and MtSKOR/GORK in the cells of *M. truncatula* root nodules. (A–C) Confocal imaging of the GFP-fused protein MtAKT1 in roots and nodules from transgenic roots carrying the construct *ProMtAKT1:MtAKT1:GFP*. (A) MtAKT1 (green fluorescence) in the root meristem was detected in the plasma membrane. Note the strong signal in the plasma membrane between the freshly divided cells (*). (B) Distal infection zone (close to the meristem), MtAKT1 was detected in the plasma membrane. Note the infection threads. Rhizobia were counterstained with propidium iodide (red). (C) MtAKT1 in the mature infected zone, the signal was visible as green dots (arrow) in the cytoplasm of infected cells, but not in the plasma membrane; in contrast to infected cells, the non-infected cells showed the signal over the plasma membrane. (D–F) Immunolocalization of MtSKOR/GORK by anti-SKOR antibody in root nodules. (D) Apical part of the root nodule and infection zone. The signal for MtSKOR/GORK (green) was present in the plasma membrane region in non-infected cells. Rhizobia were counterstained with propidium iodide (red). (E) Mature part of the nodule. Note the MtSKOR/GORK signal in the plasma membrane region of non-infected cells (arrowhead) versus the nearly absent signal in the plasma membrane of infected cells. Strong green labelling in the symbiosome membranes. (F) Magnification of infected cells. MtSKOR/GORK labelling in the symbiosome membrane (arrowhead). (G) Double localization of MtAKT1 (red fluorescence) and the endosome marker Rab7 (green fluorescence) in mature infected cells. Rhizobia were not counterstained. Note the same pattern of MtAKT1 (red dots) distribution in the cytoplasm as in (C) where MtAKT1 was displayed as green dots. The green signal for the endosomal marker Rab7 was present as very small dots encompassing individual symbiosomes. Co-localization of green and red signals provided a yellow signal in the endosomes (arrow). IC, infected cell; IT, infection thread; M, meristem; NI, non-infected cell. Scale bars: (A) 10 μm; (B) 12.5 μm; (C) 25 μm; (D) 25 μm; (E–G) 10 μm.

It is a reasonable assumption that the maintenance of an intracellular bacterial colony has its cost, and may have a detrimental effect on the host cell. Based on the high sensitivity of the root nodule to ionic stresses, we hypothesized that the infected nodule cells might have physiological defects in maintaining their ionic balance. In the present study, we describe a new aspect of the development of symbiosis: the eventual decrease of K^+ during the infected cell's life span and the putative reasons for such loss.

K^+ is one of the main players in maintaining osmotic pressure, water potential, and turgor in plant cells (Lebaudy *et al.*, 2007; Honsbein *et al.*, 2011; Shabala and Shabala, 2011). Drastic loss of K^+ is one of the symptoms of stress caused by pathogen elicitors, heavy metals, reactive oxygen species (ROS), salinity, and drought (Demidchik *et al.*, 2014; Shabala and Potosin, 2014). The loss of K^+ leads to the activation of cytosolic endonucleases that in other conditions are inhibited by this ion (Seon and J-Eun, 2002; Demidchik *et al.*, 2010). We should

Table 1. Estimation of the fluorescence signal levels for MtAKT1 and MtSKOR/GORK by ImageJ multipoint analysis of brightness on the plasma membrane region

	MtAKT1	MtSKOR/GORK	Level of autofluorescence
Non-infected cell	94.2±5.3*	93.5±1.6*	30±2.9
Infected cell	33.7±3.4*	35.6±2.9*	

Data represent means ±SD (n=10 cells, 45 dots per cell).
The difference in the level of signal over the plasma membrane region of infected and non-infected cells is significant with *P<0.01.

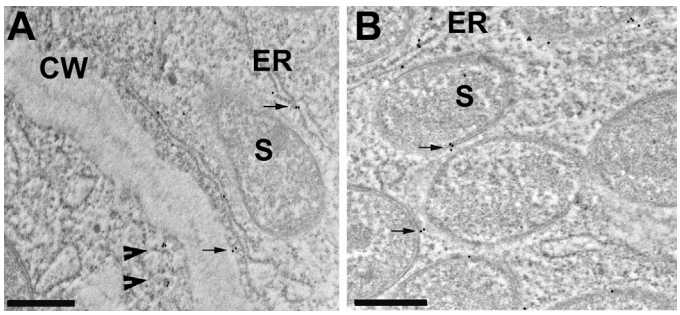

Fig. 5. Electron microscopy analysis of localization of MtAKT1 and MtSKOR/GORK by immunogold labelling. (A) Immunolabelling of MtAKT1 performed in transgenic nodules carrying the construct *ProMtAKT1:MtAKT1:GFP*. The immunosignal is revealed by anti-GFP antibody. Note the immunogold particles (arrow) over the endoplasmic reticulum (ER), the plasma membrane region surrounding the cell wall, and in the endosomes (arrowhead). (B) Immunolabelling of MtSKOR/GORK. The signal was revealed by custom-made anti-SKOR antibody. Note the gold particles over the ER and the symbiosome membranes (arrow). CW, cell wall; ER, endoplasmic reticulum; S, symbiosome; VB, vascular bundles. Scale bars: (A, B) 1µm.

point out that stress-induced K^+ leakage reaction is quite rapid, induced in minutes, lasts around 1 h, and terminates in programmed cell death (PCD; Atkinson *et al.*, 1990; Demidchik, 2014).

However, according to our results (Fig. 1C), in contrast to the stress reaction described above, in root nodules the decrease of K^+ happens gradually within 12–15 d after the release of rhizobia into the host cell, as observed in infected cells. During the life span of infected cells, K^+ diminished 3–5 times in vacuoles and symbiosomes. The reasons for such a drastic loss are complex. The pool of K^+ in infected cells should be shared between two partners, the host plant cell and several thousand bacteria that reside inside host cells. Rhizobia need K^+ for the maintenance of the osmotic status and turgor, cation/anion balancing, and control of membrane polarization (Domínguez-Ferreras *et al.*, 2009). According to our data, the level of K^+ diminishes within 6–7 cell layers (6–7 d after release from infection threads) in the nitrogen fixation zone (z3), as is shown by the low level of K^+ in mature symbiosomes. The vacuolar pool of K^+ becomes mostly exhausted in the senescence zone, situated in 12–15 cell layers. In nodules, infected cells display the earliest signs of senescence, and infected cells degenerate before non-infected cells (Pérez Guerra *et al.*, 2010). The loss of K^+ may cause the activation of cytosolic endonucleases in mature infected cells and eventually promote the so-called 'senescence' of symbiosomes and rapid termination of symbiosis. In non-infected cells, the level of K^+ was stable and they do not undergo premature senescence. The reasons for such a scenario may depend on the functional status, expression, and localization of the proteins involved in the inward or outward transport of K^+ in legume nodules. As a first study in this context, we analysed the homologues of two of the main K^+ channels in plants, the inwardly rectifying K^+ channel AKT1 and the outward-rectifying K^+ channel SKOR, in *M. truncatula*.

In this work, gene homologues of the channels *AtAKT1*, *AtSKOR*, and *AtGORK* were identified in the genomes of *M. truncatula* and other sequenced legumes. Phylogenetic analyses allowed us to characterize these homologues (Fig. 2). Legume *AKT1* homologues clustered in one clade. Legume *SKOR/GORK* homologues clustered in two clades (I and II). Only one *AKT1* and one *SKOR/GORK* homologue were identified in the genome of *M. truncatula*, as was previously reported (Damiani *et al.*, 2016; Drain *et al.*, 2020). We observed the same event in other legumes (*P. vulgaris*, *L. japonicus*, and *P. sativum*, among others). In the case of *A. hypogaea*, *L. angustifolius*, and *Glycine* sp., two *AKT1* homologues and two *SKOR/GORK* homologues of clade I were identified. Rehman *et al.* (2017) identified these *AKT1* and *SKOR/GORK* homologues in *G. max*. These results are consistent with the documented genome evolution of these species. The presence of two gene loci in *A. hypogaea* is in agreement with the recent hybrid origin of this allotetraploid species (Bertioli *et al.*, 2019). On the other hand, additional whole-genome duplications took place during the evolution of the *Lupinus* and *Glycine* lineages, not shared by other Papilionoideae (Schmutz *et al.*, 2010; Wang *et al.*, 2015; Hane *et al.*, 2017; Rehman *et al.*, 2017). Interestingly, Rehman *et al.* (2017) proposed that one *AKT1* homologue and the two soybean *SKOR/GORK* homologues of clade I are involved in nodule development.

In addition, our phylogenetic analysis showed a second clade of *SKOR/GORK*-like homologues in legumes (clade II, Fig. 2). These homologues were present in the genomes of the studied tropical legumes (*Arachis*, *Vigna*, *Cajanus*, and *Glycine*), with the exception of *Phaseolus*. These homologues were not found in the genomes of the studied temperate legumes (*Medicago*, *Lupinus*, *Pisum*, *Trifolium*, *Cicer*, and *Lotus*). These observations suggest that gene loss events of *SKOR/GORK*-like homologues from clade II occurred during the evolution of different legume lineages. Lineage-specific gene loss events during plant evolution have been reported, and some putative evolutionary implications for symbiotic relations have been suggested (Lin *et al.*, 2014; Gu *et al.*, 2016; van Velzen *et al.*, 2018). There is little information on the functional characterization of any of these legume homologues of clade II. It is interesting to note that the *G. max SKOR/GORK* homologue of clade II is not apparently involved in nodule development, as

Rehman *et al.* (2017) did not report its differential expression linked to nodulation.

The expression of both channels, MtAKT1 and MtSKOR/GORK, was detected (Fig. 3) in *M. truncatula* nodules (this work; Drain *et al.*, 2020), which is explained by the fact that the root developmental programme is co-opted for nodule formation (Franssen *et al.*, 2015). However, as our data showed, the expression of channels MtAKT1 and MtSKOR/GORK is not a guarantee that their predicted functional role will be performed. According to the analysis of protein localization (Figs 4, 5; Table 1), both channel proteins were mistargeted in infected cells and partly depleted from the plasma membrane, and MtSKOR/GORK was retargeted towards the symbiosome membrane. Previously, we reported the retargeting towards the symbiosome membrane of several proteins (Limpens *et al.*, 2009; Ivanov *et al.*, 2012; Gavrin *et al.*, 2014, 2016, 2017; Coba de la Peña *et al.*, 2018). These changes were found to be positive for the maintenance and the propagation of bacterial symbionts, but the consequences for the host cell itself were not estimated. However, in the present study when analysing the ion distribution in both infected and non-infected cells, we came across some effects, probably caused by the presence of bacteria in host cells, which resulted in the drastic changes in K^+ accessibility for the host cell housing mature nitrogen-fixing bacteria. The partial depletion of the inward channel MtAKT1 from the plams membrane of infected cells cannot but adversely affect its functional activity and inward K^+ transport. In fact, the decrease of the AKT1 labelling signal in the plasma membrane can be observed prior to the decrease of K^+ content in the vacuoles, as these two events occur in z2 and z3, and in z4, respectively. We can speculate that the low level of the outward channel MtSKOR/GORK in the plasma membrane in infected cells, in contrast to that of MtAKT1, may have a compensatory effect for host cell survival in such harsh situations, because it can prevent the further loss of K^+ from the cell. The *AtGORK* mutant of *A. thaliana*, lacking a functional K^+ efflux channel, showed less damage under salinity stress conditions than the wild-type control (Demidchik *et al.*, 2010). However, the location of MtSKOR/GORK in the symbiosome membrane may contribute to the K^+ decrease observed in symbiosomes. The goal for a further study should be to find out the reasons for the mistargeting and the depletion of these channels in the plasma membrane in mature infected cells. One of the reasons for the incorrect incorporation of proteins into the plasma membrane might be the drastic changes in the actin cytoskeleton conformation found in nodule-infected cells as compared with non-infected cells, that may negatively affect the correct targeting of the vesicles (Fedorova *et al.*, 2007; Gavrin *et al.*, 2015). The existence of a mechanism coordinating SNARE-mediated vesicle trafficking and ion transport engaging directly with a subset of K^+ channels, which has been identified in *A. thaliana* (Honsbein *et al.*, 2009; Karnik *et al.*, 2017), provides direction for further research of the process.

Nodule development is the result of selection, evolution, and also gene duplication (van Velzen *et al.*,2018). Evolution has given to legumes and rhizobia the ability to form an integral unit, the root nodule. However, the intracellular lifestyle of symbiotic bacteria affects the host cell. Symbiotic infected cells sustain a huge bacterial colony, and several physiological differences/changes in the infected cell have to be produced to allow it, as compared with nodule-non-infected cells. The changes in the host cell include, among others, membrane traffic and protein retargeting, as we have previously reported, such as the relocation of proteins of the SNARE group and small GTPases, which regulate the membrane fusion (Limpens *et al.*, 2009; Ivanov *et al.*, 2012; Gavrin *et al.*, 2016), changes in the vacuolar system of infected cells and the relocation of aquaporins (Gavrin *et al.*, 2014), rearrangements of the cytoskeleton conformation, and relocation of proteins involved in actin formation to the symbiosome membrane (Fedorova *et al.*, 2007; Gavrin *et al.*, 2015). Infected cell membrane trafficking is one of the main factors for the maintenance of symbiotic bacteria in the host cell.

Now, in this work, we have reported a new aspect in membrane trafficking and protein targeting in nodule-infected cells: mistargeting and partial depletion of the K^+ channels MtAKT1 and MtSKOR/GORK from the plasma membrane. A clear mislocation of both channels was found in infected cells, as compared with non-infected cells. The mislocation of the channels is an event that might depend on changes in the cytoskeleton pattern, which in turn depends on the presence of bacteria in the symplast of infected cells.

Apart from the role of these channels in K^+ transport, they may have important functions in stress response, because not only a cytosolic K^+/Na^+ ratio, but also absolute concentrations of K^+ are essential to confer stress tolerance (Sharma *et al.*, 2013; Wu *et al.*, 2018; Adem *et al.*, 2020). The outward-rectifying channel GORK is involved in stress-induced K^+ loss from the cytosol (Adem *et al.*, 2020), and modulates plant responses to abscisic acid (Lim *et al.*, 2019). ROS are able to activate GORK and increase the loss of K^+ (Demidchik *et al.*, 2010). In the case of salinity stress, the deficiency of K^+ in root cells can be compensated from the vacuolar pool, but, after this source is exhausted, cytosolic K^+ declines below a certain threshold, and triggers PCD by activating caspase-like proteases and endonucleases (Adem *et al.*, 2020). The data on the progressive decrease in K^+ content in the vacuoles of infected cells support this scenario. According to IDA, in the senescence zone, the level of K^+ in the vacuoles drastically diminished. It should be noted that hypoxia negatively affects K^+ availability in plant roots (Gill *et al.*, 2017; Wang *et al.*, 2017), and the root nodule is forming a hypoxic environment. Nodules also show the presence of ROS (Andrio *et al.*, 2013; Puppo *et al.*, 2013; Montiel *et al.*, 2016), which are major activators of K^+ efflux by SKOR (Demidchik, 2018). Nodules need a fine-tuning of the K^+ balance, and our results suggest that this ion homeostasis might differ between infected and non-infected cells and it might contribute to the short life span of infected cells.

In conclusion, in this work we have reported remarkable differences in K^+ content and location of the channels MtAKT1 and MtSKOR/GORK between infected and uninfected nodule cells, which might compromise K^+ availability and have physiological consequences for the host cell. We propose that *M. truncatula* nodule-infected cells do have alterations in K^+ availability, as compared with non-infected cells, probably due to the high demand of intracellular rhizobia and the flaws in the location of the proteins of the host plant K^+ channels MtAKT1 and MtSKOR/GORK. The reduction of K^+ levels in the host cell, and in the microsymbiont itself, might negatively affect the life span of the infected cells and the ability of the symbiotic tissue to withstand stress. Analyses of *M. truncatula* lines overexpressing or silencing these channel genes might provide further insight into the mechanisms related to the events described here and their putative role in senescence, ionic stress responses, and other nodule physiological processes. Therefore, the special features of infected cell K^+ transport need to be taken into consideration in studies aimed to improve the stress tolerance of root nodules.

Supplementary data

The following supplementary data are available at *JXB* online.

Table S1. List of primers used in this research.

Table S2. Relative distribution of elements in *Medicago truncatula* nodules.

Fig. S1. Putative functional domains of MtAK1 and MtSKOR/GORK proteins, predicted with the SMART tool.

Fig. S2. Structural features of the N-terminal region of MtAKT1.

Fig. S3. Structural features of the N-terminal region of MtSKOR/GORK.

Fig. S4. Single channel confocal images of the immunolocalization of MtAKT1 and MtSKOR/MtGORK shown in Fig. 4C and F.

Fig. S5. Western blot analysis of MtSKOR/GORK antigens in plasma membrane of *M. truncatula* roots with anti-MtSKOR antibody.

Acknowledgements

This article is dedicated to our late friend Fernando Pinto, technician of the Electron Microscopy Service in ICA. The authors are very grateful to Dr Henk Franssen for critical reading and editing of the manuscript. The work was supported by the RFBR (Russian Foundation for Basic Research, grant 19-04-00570 to EEF), Comunidad de Madrid (grant S2009/AMB-151 to MML), MINECO (grant AGL2013-40758-R to JJP and MML), AEI/FEDER-UE (grant AGL2017-88381-R to JJP and MML), Spanish Ministery of Education (sabbatical year contract ref. SAB2010-0086 to EEF), and MINECO (predoctoral contract ref. BES-014-069558 to VL-D). EEF also thanks the Ministry of Science and Higher Education of the Russian Federation for covering the basic supplies for the research (0087-2019-0013). We acknowledge support of the publication fee by the CSIC Open Access Publication Support Initiative through its Unit of Information Resources for Research (URICI).

Author contributions

EEF, TCP, and MML designed the research; EEF, VL-D, TCP, NAT, OK, JJP, and MML performed experiments and analysed data; EEF, TCP, and MML wrote the manuscript; EEF, TCP, OK, JJP, and MML edited the manuscript.

The authors have no conflict of interest to declare.

Data availability

The raw data supporting the results reported in this article will be made available from the corresponding authors on request, without reservation.

References

Adem GD, Chen G, Shabala L, Chen ZH, Shabala S. 2020. GORK channel: a master switch of plant metabolism? Trends in Plant Science **25**, 434–445.

Andrio E, Marino D, Marmeys A, de Segonzac MD, Damiani I, Genre A, Huguet S, Frendo P, Puppo A, Pauly N. 2013. Hydrogen peroxide-regulated genes in the *Medicago truncatula–Sinorhizobium meliloti* symbiosis. New Phytologist **198**, 179–189.

Atkinson MM, Keppler LD, Orlandi EW, Baker CJ, Mischke CF. 1990. Involvement of plasma membrane calcium influx in bacterial induction of the K/H and hypersensitive responses in tobacco. Plant Physiology **92**, 215–221.

Benedito VA, Li H, Dai X, *et al.* 2010. Genomic inventory and transcriptional analysis of *Medicago truncatula* transporters. Plant Physiology **152**, 1716–1730.

Bertioli DJ, Jenkins J, Clevenger J, *et al.* 2019. The genome sequence of segmental allotetraploid peanut *Arachis hypogaea*. Nature Genetics **51**, 877–884.

Bertrand A, Bipfubusa M, Dhont C, Chalifour FP, Drouin P, Beauchamp CJ. 2016. Rhizobial strains exert a major effect on the amino acid composition of alfalfa nodules under NaCl stress. Plant Physiology and Biochemistry **108**, 344–352.

Coba de la Peña T, Cárcamo CB, Almonacid L, Zaballos A, Lucas MM, Balomenos D, Pueyo JJ. 2008. A salt stress-responsive cytokinin receptor homologue isolated from *Medicago sativa* nodules. Planta **227**, 769–779.

Coba de la Peña T, Fedorova E, Pueyo JJ, Lucas MM. 2018. The symbiosome: legume and rhizobia co-evolution toward a nitrogen-fixing organelle? Frontiers in Plant Science **8**, 2229.

Coba de la Peña T, Pueyo JJ. 2012. Legumes in the reclamation of marginal soils, from cultivar and inoculant selection to transgenic approaches. Agronomy for Sustainable Development **32**, 65–91.

Coskun D, Kronzucker HJ. 2013. Complexity of potassium acquisition: how much flows through channels? Plant Signaling & Behavior **8**, e24799.

Damiani I, Drain A, Guichard M, *et al.* 2016. Nod factor effects on root hair-specific transcriptome of *Medicago truncatula:* focus on plasma membrane transport systems and reactive oxygen species networks. Frontiers in Plant Science **7**, 794.

Demidchik V. 2014. Mechanisms and physiological roles of K^+ efflux from root cells. Journal of Plant Physiology **171**, 696–707.

Demidchik V. 2018. ROS-activated ion channels in plants: biophysical characteristics, physiological functions and molecular nature. International Journal of Molecular Sciences **19**, 1263.

Demidchik V, Cuin TA, Svistunenko D, Smith SJ, Miller AJ, Shabala S, Sokolik A, Yurin V. 2010. Arabidopsis root K^+-efflux conductance activated by hydroxyl radicals: single-channel properties, genetic basis and

involvement in stress-induced cell death. Journal of Cell Science **123**, 1468–1479.

Demidchik V, Straltsova D, Medvedev SS, Pozhvanov GA, Sokolik A, Yurin V. 2014. Stress-induced electrolyte leakage: the role of K^+-permeable channels and involvement in programmed cell death and metabolic adjustment. Journal of Experimental Botany **65**, 1259–1270.

Desbrosses G, Kopka C, Ott T, Udvardi MK. 2004. *Lotus japonicus* LjKUP is induced late during nodule development and encodes a potassium transporter of the plasma membrane. Molecular Plant-Microbe Interactions **17**, 789–797.

Domínguez-Ferreras A, Soto MJ, Pérez-Arnedo R, Olivares J, Sanjuán J. 2009. Importance of trehalose biosynthesis for *Sinorhizobium meliloti* osmotolerance and nodulation of alfalfa roots. Journal of Bacteriology **191**, 7490–7499.

Drain A, Thouin J, Wang L, Boeglin M, Pauly N, Nieves-Cordones M, Gaillard I, Véry AA, Sentenac H. 2020. Functional characterization and physiological roles of the single Shaker outward K^+ channel in *Medicago truncatula*. The Plant Journal **102**, 1249–1265.

Fedorova E, Thomson R, Whitehead LF, Maudoux O, Udvardi MK, Day DA. 1999. Localization of H^+-ATPases in soybean root nodules. Planta **209**, 25–32.

Fedorova EE, de Felipe MR, Pueyo JJ, Lucas MM. 2007. Conformation of cytoskeletal elements during the division of infected *Lupinus albus* L. nodule cells. Journal of Experimental Botany **58**, 2225–2236.

Franssen HJ, Xiao TT, Kulikova O, Wan X, Bisseling T, Scheres B, Heidstra R. 2015. Root developmental programs shape the *Medicago truncatula* nodule meristem. Development **142**, 2941–2950.

Gavrin A, Chiasson D, Ovchinnikova E, Kaiser BN, Bisseling T, Fedorova EE. 2016. VAMP721a and VAMP721d are important for pectin dynamics and release of bacteria in soybean nodules. New Phytologist **210**, 1011–1021.

Gavrin A, Jansen V, Ivanov S, Bisseling T, Fedorova E. 2015. ARP2/3-mediated actin nucleation associated with symbiosome membrane is essential for the development of symbiosomes in infected cells of *Medicago truncatula* root nodules. Molecular Plant-Microbe Interactions **28**, 605–614.

Gavrin A, Kaiser BN, Geiger D, Tyerman SD, Wen Z, Bisseling T, Fedorova EE. 2014. Adjustment of host cells for accommodation of symbiotic bacteria: vacuole defunctionalization, HOPS suppression, and TIP1g retargeting in *Medicago*. The Plant Cell **26**, 3809–3822.

Gavrin A, Kulikova O, Bisseling T, Fedorova EE. 2017. Interface symbiotic membrane formation in root nodules of *Medicago truncatula*: the role of synaptotagmins MtSyt1, MtSyt2 and MtSyt3. Frontiers in Plant Science **8**, 201.

Gaymard F, Pilot G, Lacombe B, Bouchez D, Bruneau D, Boucherez J, Michaux-Ferrière N, Thibaud JB, Sentenac H. 1998. Identification and disruption of a plant shaker-like outward channel involved in K^+ release into the xylem sap. Cell **94**, 647–655.

Gill MB, Zeng F, Shabala L, Böhm J, Zhang G, Zhou M, Shabala S. 2017. The ability to regulate voltage-gated K^+-permeable channels in the mature root epidermis is essential for waterlogging tolerance in barley. Journal of Experimental Botany **69**, 667–680.

Gu Y, Xing S, He C. 2016. Genome-wide analysis indicates lineage-specific gene loss during papilionoideae evolution. Genome Biology and Evolution **8**, 635–648.

Hane JK, Ming Y, Kamphuis LG, *et al.* 2017. A comprehensive draft genome sequence for lupin (*Lupinus angustifolius*), an emerging health food: insights into plant–microbe interactions and legume evolution. Plant Biotechnology Journal **15**, 318–330.

Hodges TK, Mills D. 1986. Isolation of plasma membrane. Methods in Enzymology **118**, 41–54.

Honsbein A, Blatt MR, Grefen C. 2011. A molecular framework for coupling cellular volume and osmotic solute transport control. Journal of Experimental Botany **62**, 2363–2370.

Honsbein A, Sokolovski S, Grefen C, Campanoni P, Pratelli R, Paneque M, Chen Z, Johansson I, Blatt MR. 2009. A tripartite SNARE–K^+ channel complex mediates in channel-dependent K^+ nutrition in Arabidopsis. The Plant Cell **21**, 2859–2877.

Ivanov S, Fedorova EE, Limpens E, De Mita S, Genre A, Bonfante P, Bisseling T. 2012. Rhizobium–legume symbiosis shares an exocytotic pathway required for arbuscule formation. Proceedings of the National Academy of Sciences, USA **109**, 8316–8321.

Johansson I, Wulfetange K, Porée F, *et al.* 2006. External K^+ modulates the activity of the Arabidopsis potassium channel SKOR via an unusual mechanism. The Plant Journal **46**, 269–281.

Karnik R, Waghmare S, Zhang B, Larson E, Lefoulon C, Gonzalez W, Blatt MR. 2017. Commandeering channel voltage sensors for secretion, cell turgor, and volume control. Trends in Plant Science **22**, 81–95.

Kelley LA, Mezulis S, Yates CM, Wass MN, Sternberg MJ. 2015. The Phyre2 web portal for protein modeling, prediction and analysis. Nature Protocols **10**, 845–858.

Kijne JW. 1975. The fine structure of pea root nodules. 2. Senescence and disintegration of the bacteroid tissue. Physiological Plant Pathology **7**, 17–21.

Kumar S, Stecher G, Li M, Knyaz C, Tamura K. 2018. MEGA X: Molecular Evolutionary genetics analysis across computing platforms. Molecular Biology and Evolution **35**, 1547–1549.

Lebaudy A, Véry AA, Sentenac H. 2007. K^+ channel activity in plants: genes, regulations and functions. FEBS letters **581**, 2357–2366.

Leidi EO, Barragán V, Rubio L, *et al.* 2010. The AtNHX1 exchanger mediates potassium compartmentation in vacuoles of transgenic tomato. The Plant Journal **61**, 495–506.

Lim CW, Kim SH, Choi HW, Luan S, Lee SC. 2019. The Shaker type potassium channel, GORK, regulates abscisic acid signaling in Arabidopsis. The Plant Pathology Journal **35**, 684–691.

Limpens E, Ivanov S, van Esse W, Voets G, Fedorova E, Bisseling T. 2009. *Medicago* N_2-fixing symbiosomes acquire the endocytic identity marker Rab7 but delay the acquisition of vacuolar identity. The Plant Cell **21**, 2811–2828.

Limpens E, Ramos J, Franken C, Raz V, Compaan B, Franssen H, Bisseling T, Geurts R. 2004. RNA interference in *Agrobacterium rhizogenes*-transformed roots of *Arabidopsis* and *Medicago truncatula*. Journal of Experimental Botany **55**, 983–992.

Lin Y, Cheng Y, Jin J, Jin X, Jiang H, Yan H, Cheng B. 2014. Genome duplication and gene loss affect the evolution of heat shock transcription factor genes in legumes. PLoS One **9**, e102825.

Long-Tang H, Li-Na Z, Li-Wei G, Anne-Aliénor V, Hervé S, Yi-Dong Z. 2018. Constitutive expression of CmSKOR, an outward K^+ channel gene from melon, in *Arabidopsis thaliana* involved in saline tolerance. Plant Science **274**, 492–502.

Meckel T, Hurst AC, Thiel G, Homann U. 2004. Endocytosis against high turgor: intact guard cells of *Vicia faba* constitutively endocytose fluorescently labelled plasma membrane and GFP-tagged K-channel KAT1. The Plant Journal **39**, 182–193.

Montiel J, Arthikala MK, Cárdenas L, Quinto C. 2016. Legume NADPH oxidases have crucial roles at different stages of nodulation. International Journal of Molecular Sciences **17**, 680.

Nei M, Kumar S. 2000. Molecular evolution and phylogenetics. Oxford University Press.

Nieves-Cordones M, Alemán F, Martínez V, Rubio F. 2014. K^+ uptake in plant roots. The systems involved, their regulation and parallels in other organisms. Journal of Plant Physiology **171**, 688–695.

Pérez Guerra JC, Coussens G, De Keyser A, De Rycke R, De Bodt S, Van De Velde W, Goormachtig S, Holsters M. 2010. Comparison of developmental and stress-induced nodule senescence in *Medicago truncatula*. Plant Physiology **152**, 1574–1584.

Pfaffl MW. 2001. A new mathematical model for relative quantification in real-time RT–PCR. Nucleic Acids Research **29**, 2002–2007.

Puppo A, Groten K, Bastian F, Carzaniga R, Soussi M, Lucas MM, de Felipe MR, Harrison J, Vanacker H, Foyer CH. 2005. Legume nodule

senescence: roles for redox and hormone signalling in the orchestration of the natural aging process. New Phytologist **165**, 683–701.

Puppo A, Pauly N, Boscari A, Mandon K, Brouquisse R. 2013. Hydrogen peroxide and nitric oxide: key regulators of the legume–*Rhizobium* and mycorrhizal symbioses. Antioxidants & Redox Signaling **18**, 2202–2219.

Ragel P, Raddatz N, Leidi EO, Quintero FJ, Pardo JM. 2019. Regulation of K^+ nutrition in plants. Frontiers in Plant Science **10**, 281.

Rehman HM, Nawaz MA, Shah ZH, Daur I, Khatoon S, Yang SH, Chung G. 2017. In-depth genomic and transcriptomic analysis of five K^+ transporter gene families in soybean confirm their differential expression for nodulation. Frontiers in Plant Science **8**, 804.

Roth LE, Stacey G. 1989. Bacterium release into host cells of nitrogen-fixing soybean nodules: the symbiosome membrane comes from three sources. European Journal of Cell Biology **49**, 13–23.

Rubio F, Nieves-Cordones M, Horie T, Shabala S. 2020. Doing 'business as usual' comes with a cost: evaluating energy cost of maintaining plant intracellular K^+ homeostasis under saline conditions. New Phytologist **225**, 1097–1104.

Schmutz J, Cannon SB, Schlueter J, *et al.* 2010. Genome sequence of the palaeopolyploid soybean. Nature **463**, 178–183.

Schneider CA, Rasband WS, Eliceiri KW. 2012. NIH Image to ImageJ: 25 years of image analysis. Nature Methods **9**, 671–675.

Seon P, Ja-Eun K. 2002. Potassium efflux during apoptosis. Journal of Biochemistry and Molecular Biology **35**, 41–46.

Shabala S, Pottosin I. 2014. Regulation of potassium transport in plants under hostile conditions: implications for abiotic and biotic stress tolerance. Physiologia Plantarum **151**, 257–279.

Shabala S, Shabala L. 2011. Ion transport and osmotic adjustment in plants and bacteria. Biomolecular Concepts **2**, 407–419.

Sharma T, Dreyer I, Riedelsberger J. 2013. The role of K^+ channels in uptake and redistribution of potassium in the model plant *Arabidopsis thaliana*. Frontiers in Plant Science **4**, 224.

Shvaleva A, Coba de la Peña T, Rincón A, Morcillo CN, García de la Torre VS, Lucas MM, Pueyo JJ. 2010. Flavodoxin overexpression reduces cadmium-induced damage in alfalfa root nodules. Plant and Soil **326**, 109–121.

Smit P, Raedts J, Portyanko V, Debellé F, Gough C, Bisseling T, Geurts R. 2005. NSP1 of the GRAS protein family is essential for rhizobial Nod factor-induced transcription. Science **308**, 1789–1791.

Tamura K, Nei M. 1993. Estimation of the number of nucleotide substitutions in the control region of mitochondrial DNA in humans and chimpanzees. Molecular Biology and Evolution **10**, 512–526.

Torres MJ, Rubia MI, de la Peña TC, Pueyo JJ, Bedmar EJ, Delgado MJ. 2014. Genetic basis for denitrification in *Ensifer meliloti*. BMC Microbiology **14**, 142.

Tsyganov VE, Belimov AA, Borisov AY, Safronova VI, Georgi M, Dietz KJ, Tikhonovich IA. 2007. A chemically induced new pea (*Pisum sativum*) mutant SGECdt with increased tolerance to, and accumulation of, cadmium. Annals of Botany **99**, 227–237.

Udvardi M, Poole PS. 2013. Transport and metabolism in legume–rhizobia symbioses. Annual Review of Plant Biology **64**, 781–805.

Untergasser A, Nijveen H, Rao X, Bisseling T, Geurts R, Leunissen JA. 2007. Primer3Plus, an enhanced web interface to Primer3. Nucleic Acids Research **35**, W71–W74.

van Velzen R, Holmer R, Bu F, *et al.* 2018. Comparative genomics of the nonlegume *Parasponia* reveals insights into evolution of nitrogen-fixing *Rhizobium* symbioses. Proceedings of the National Academy of Sciences, USA **115**, E4700–E4709.

Vasse J, de Billy F, Camut S, Truchet G. 1990. Correlation between ultrastructural differentiation of bacteroids and nitrogen fixation in alfalfa nodules. Journal of Bacteriology **172**, 4295–4306.

Verdier J, Kakar K, Gallardo K, Le Signor C, Aubert G, Schlereth A, Town CD, Udvardi MK, Thompson RD. 2008. Gene expression profiling of *M. truncatula* transcription factors identifies putative regulators of grain legume seed filling. Plant Molecular Biology **67**, 567–580.

Véry AA, Nieves-Cordones M, Daly M, Khan I, Fizames C, Sentenac H. 2014. Molecular biology of K^+ transport across the plant cell membrane: what do we learn from comparison between plant species? Journal of Plant Physiology **171**, 748–769.

Wang F, Chen ZH, Shabala S. 2017. Hypoxia sensing in plants: on a quest for ion channels a putative oxygen sensors. Plant & Cell Physiology **58**, 1126–1142.

Wang J, Andersen SU, Ratet P. 2018. Editorial: Molecular and cellular mechanisms of the legume–rhizobia symbiosis. Frontiers in Plant Science **9**, 1839.

Wang Y, Wu WH. 2013. Potassium transport and signaling in higher plants. Annual Review of Plant Biology **64**, 451–476.

Wang Z, Cheng K, Wan L, Yan L, Jiang H, Liu S, Lei Y, Liao B. 2015. Genome-wide analysis of the basic leucine zipper (bZIP) transcription factor gene family in six legume genomes. BMC Genomics **16**, 1053.

Wu H, Zhang X, Giraldo JP, Shabala S. 2018. It is not all about sodium: revealing tissue specificity and signalling roles of potassium in plant responses to salt stress. Plant and Soil **431**, 1–17.

Yang S, Wang Q, Fedorova E, *et al.* 2017. Microsymbiont discrimination mediated by a host-secreted peptide in *Medicago truncatula*. Proceedings of the National Academy of Sciences, USA **114**, 6848–6853.

Zahran HH. 1999. *Rhizobium*–legume symbiosis and nitrogen fixation under severe conditions and in an arid climate. Microbiology and Molecular Biology Reviews **63**, 968–989.